위상 확장 디콘볼루션 방식을 이용한 SAR 영상 향상

도대원, 송우진, 권준찬

포항공과대학교 전자컴퓨터공학부 전자파연구센터

SAR IMAGE ENHANCEMENT BASED ON THE PHASE EXTENSION DECONVOLUTION METHOD

Dae-Won Do, Woo-Jin Song and Jun-Chan Kwon

Microwave Application Research Center, Division of Electronics & Computer Engineering
Pohang University of Science and Technology

ABSTRACT

In this paper, we propose a novel post processing method of deconvolution for SAR images based on phase extension inverse filtering, which improves spatial resolution as well as effectively eliminates sidelobes with low computational complexity. It extends the bandwidth only to control the magnitude of the processed SAR data without distortions of the phase in frequency domain unlike the other techniques such as spatially variant apodization (SVA), and other deconvolution techniques. We compare the image processed by the proposed method with images processed by uniform weighting function, Hamming weighting function whose coefficient is 0.75, and SVA

1. INTRODUCTION

Due to the capability of producing high-resolution imagery from data collected by a relatively small antenna, synthetic aperture radar (SAR) has been used for various purposes [1]. Conventionally, SAR images are reconstructed from raw data by matched filtering. In this method, the one-dimensional process is applied twice on the raw data expressed in two dimensions, the range and azimuth directions [2]. While the impulse response obtained by the matched filter approach produces the best achievable signal-to-noise ratio, large sidelobes are to be reduced for obtaining high-resolution SAR images.

Applying amplitude weighting functions to the data prior to final FFT has traditionally reduced sidelobes such as Hamming weighting function. These weighting methods, however, can achieve the lower sidelobes at the expense of the mainlobe width, which results in degradation of resolution. So recently super-resolution techniques [3], such as adaptive sidelobe reduction (ASR) [4], super spatially variant apodization (Super-SVA) [5], adaptive FIR filtering approaches [6] were proposed to reduce the sidelobes without degradation of resolution. These super-resolution techniques have been traditionally limited to problems where *a-priori* knowledge of scene content is available, the scene content is suitably constrained and/or the large computational complexity is needed.

To enhance the resolution beyond the matched filter classical limit, we present phase extension inverse filtering as a deconvolution of SAR imagery. This method improves spatial resolutions as well as effectively eliminates side-lobes with low computational complexity.

The rest of this paper is organized as follows. Section 2 reviews the conventional matched filter approach. In Section 3, we formulate phase extension inverse filtering method. Section 4 presents a simulated SAR image processed by the proposed method comparing them with the images processed by other techniques. Finally, Section 5 presents a summary and conclusions.

2. CHARACTERISTICS OF MATCHED FILTERING IN SAR IMAGING

For simplicity, consider the one-dimensional geometry shown in Fig. 1. An antenna located at the origin illuminates point-like scatter centered at $x = R$, having reflectivity $q(x) = m(x)\exp[j\psi(x)]$. Let the transmitted signal, $\bar{s}(t)$ be a linear FM pulse of duration τ_p and bandwidth $B = K\tau_p$.

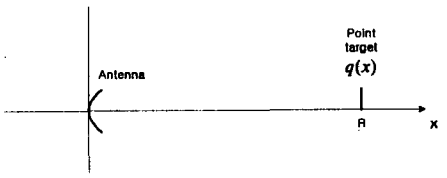

Fig. 1. Simplified SAR geometry

$$\bar{s}(t) = \exp\left[j2\pi\left(f_c t + Kt^2/2\right)\right], \quad |t| < \tau_p \\ = s(t)\exp[j2\pi f_c t] \tag{1}$$

where

$$s(t) = \exp\left[j\pi Kt^2\right], \quad |t| < \tau_p . \tag{2}$$

In the band, for large $B\tau_p$ the approximation for $S(f)$, the spectrum of $s(t)$, results:

$$S(f) = |K|^{-1} \exp[j(\pi/4)\mathrm{sgn}(K)]\exp[-j\pi f^2/K] \quad \text{where } |f| < B/2. \tag{3}$$

Fig. 2 shows the FFT of $s(t)$, where the parameters of linear FM pulse are set as $\tau_p = 32\mu\,\mathrm{sec}$, $B = 15.5MHz$, $B\tau_p \approx 500$ and the sampling frequency, f_s, is $18.96MHz$.

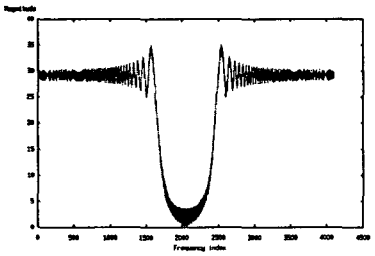

(a) Magnitude plot of $S(f)$

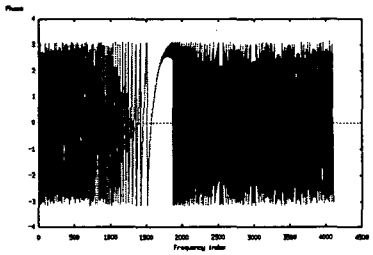

(b) Phase plot of $S(f)$

Fig. 2. $S(f)$, FFT plots of $s(t)$.

Consider the case of a deterministic "point" radar reflector, i.e. $q(x) = \delta(R)$, in a zero clutter background with zero receiver noise. Then received signal is given by

$$v_r(t) = \bar{s}(t - 2R/c). \tag{4}$$

An estimate of the reflectivity can be obtained by processing $v_r(t)$ with a matched filter whose impulse response is $p(t) = \bar{s}^*(-t)$. Therefore, the demodulated estimate of the reflectivity can be expressed in frequency domain as

$$\begin{aligned} H(f) &= \{V_r(f)P(f)\} \otimes \delta(f - f_c) \\ &= S^*(f)S(f)\exp[-j2\pi f_c R/c] \\ &= |S(f)|^2 \exp[-j2\pi f_c R/c]. \end{aligned} \tag{5}$$

If $|S(f)|^2$ is rectangular, as is the case in particular for $s(t)$ a linear FM pulse with $B\tau_p > 100$, then $H(f)$ is supposed to have a rectangular amplitude spectrum with bandwidth B. So, the impulse response of $h(t)$ can be expressed as approximation Eq. (6).

$$\begin{aligned} h(t) &\approx \exp[-j2\pi f_c R/c]\mathrm{sinc}(u) \\ u &= \pi K \tau_p (t - 2R/c) \end{aligned} \tag{6}$$

where $\mathrm{sinc}(u) \equiv \sin(u)/u$, and therefore, the resolution is given by

$$\delta R = c/2B \tag{7}$$

from the approximation, $s(t) \otimes s^*(-t) \approx \mathrm{sinc}(u)$. Fig. 3 shows the sinc-like magnitude of impulse response, $h(t)$, for point target without background noise, which is normalized. Fig. 4 shows the frequency transfer function, $H(f)$, for Fig. 3.

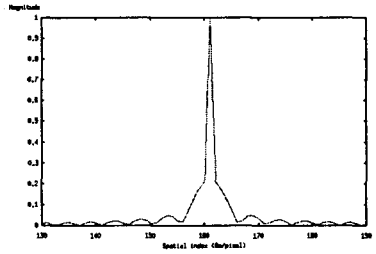

Fig. 3. Magnitude of impulse response, $h(t)$.

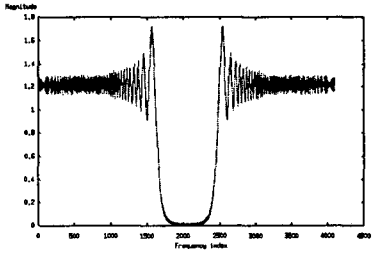

(a) Magnitude plot

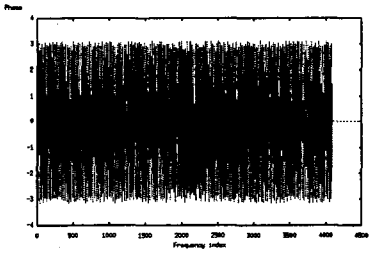

(b) Phase plot

Fig. 4. Frequency transfer function, $H(f)$.

3. PHASE EXTENSION DECONVOLUTION FORMULATION

With the impulse response, traditional inverse filtering expressed in (8) has a problem in extending the bandwidth of SAR data to enhance a spatial resolution, and SVA [7] can

extend the bandwidth but phase distortions occur as results of extending the bandwidth.

$$\hat{X}(u,v)=\begin{cases}\dfrac{\tilde{X}(u,v)}{H(u,v)} & where\ |H(u,v)|>T\\ 0.0, & elsewhere\end{cases} \tag{8}$$

Here we can divide the frequency domain of $|H(u,v)|$ according to a threshold value (T) chosen as in Fig. 3. The domain 1 in Fig. 5 represents the frequency domain of original band-limited signal, which determines the spatial resolution of SAR image. To enhance the spatial resolution, we can extend the frequency domain greater than the original band-limited signal. Domain 2 represents the extended bandwidth.

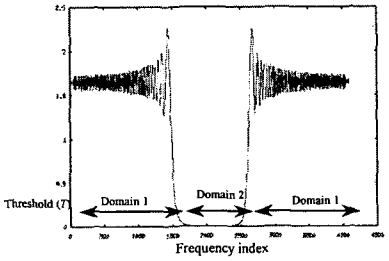

Fig. 5. Division of domain in $|H(u,v)|$

According to the domains in Fig. 5, phase extension inverse filtering is formulated as follows:

$$\hat{X}(u,v)=\begin{cases}\dfrac{\tilde{X}(u,v)}{|H(u,v)|}, & \text{if } |H(u,v)|>T\\ \dfrac{\tilde{X}(u,v)}{|\tilde{X}(u,v)|}\times\eta C, & \text{if } |H(u,v)|<T, |\tilde{X}(u,v)|>\sigma\\ 0.0, & elsewhere,\end{cases} \tag{9}$$

where η is a system parameter which controls the magnitude of the processed SAR data $\tilde{X}(u,v)$ in the extended band, σ is a control parameter for computational precision, and C is the square root of signal energy which is defined by

$$C=\sqrt{\sum_{i=0}^{N-1}\sum_{j=0}^{M-1}|\tilde{x}(i,j)|^2}, \tag{10}$$

where M,N represent the image sizes of each direction of azimuth and range in spatial domain. Note that if the variance of the noise $n(i,j)$ added to the received SAR raw data increases, the value of C expressed in (10) also increases. So, we have to control the magnitude in the extended band with the system parameter η to prevent the effect of the added noise from being larger than that of the desired signal of reflectivity.

The value of η is set to be inversely proportional to the variance of the added noise. The relation between η and the noise can be expressed as

$$\eta=\frac{K}{\mathrm{var}\{n(i,j)\}}, \tag{11}$$

where K is an inverse ratio which is chosen empirically.

As indicated in (5), the phase extension inverse filtering extends the bandwidth only to control the magnitude of the processed SAR data $\tilde{X}(u,v)$ without affecting the phase of that. Since the phase distortions in the frequency domain correspond to displacements in the spatial domain, they may degrade the spatial resolutions. However, phase extension inverse filtering retains the phase of the processed SAR data and extends the bandwidth with only controlling the magnitude, it does not cause phase distortions. In domain 1, we control the magnitude as a concept of ideal filtering. And in domain 2, we adjust the power level to improve the spatial resolutions.

In Section 4, we verify the performance of the phase extension inverse filtering method through simulation.

4. SIMULATION

In order to verify the performance of the proposed method, simulation of the ERS-1 mission whose general parameters are given in Table 1 was carried out.

Orbital altitude	785 (km)
Look angle	20.3 (degrees)
Incidence angle	23.0 (degrees)
Azimuth antenna dimension	10 (m)
Range antenna dimension	1 (m)
Frequency	5.3 (GHz)
Chirp bandwidth	15.5 (MHz)
A/D sampling rate	18.96 (Msamples/sec)
Pulse Repetition Frequency (PRF)	1680 (Hz)
Pulse duration	37.1 (μs)
Azimuth image pixel spacing	3.981 (m)
Range image pixel spacing	7.904 (m)

Table 1. ERS parameters used in the simulation runs

Fig. 6 (a) is a reflectivity map used in the simulation, and all magnitudes of 77 targets in Fig. 6 (a) are set as 1. Fig. 6 (b) is the received raw data which is corrupted by additive white Gaussian noise with variance 0.25. Each image displayed in this paper is scaled to make its maximum 255. To analyze the effect of the additive noise in the receiver, the mean power of the raw data without noise is calculated by

$$\varepsilon_t=\sum_{A_p}\sum E\{|v_r(i,j)|\}, \tag{12}$$

where A_p represents a area in which the signal returned by targets exists. And receiver noise power is calculated by

(a) Reflectivity map (b) Received raw data

Fig. 6. SAR simulation data

$$\varepsilon_n = \sum_{A_n} \sum E\{|n(i,j)|\}, \quad (13)$$

where A_n is a area in which noise affect the return signal, and we set $A_n = A_p$. Now, we define the signal-to-noise ratio (SNR) of the raw data as follows.

$$SNR_{raw} = 20\log_{10}\frac{\varepsilon_t}{\varepsilon_n}(dB). \quad (14)$$

So, the SNR_{raw} of the raw data used in the simulation is 18.84 dB. Fig. 7 compares the image processed by the proposed method with images processed by uniform weighting function, Hamming weighting function whose coefficient is 0.75, and SVA. In Fig. 7 (d), the parameters of the proposed filter in (9) are set such as the threshold (T) is 0.1, the system parameter (η) is 0.8, and the control parameter (σ) is 0.000001.

Note that the phase extension inverse filtering improves spatial resolution as well as effectively eliminates sidelobes more than other techniques. Also note that the computational complexity of the proposed method is low because it needs only the scaling of magnitude in the frequency domain and no iterations.

5. SUMMARY AND CONCLUSIONS

The phase extension inverse filtering is introduced which improves spatial resolution as well as effectively eliminates sidelobes with low computational complexity. It extends the bandwidth only to control the magnitude of the processed SAR data without distortions of the phase information in frequency domain.

The performance of the proposed method is verified through the simulation in Section 4. Note that applying it to the real SAR image with refined Doppler parameters, Doppler centroid and Doppler frequency rate, will be a subject of future works.

6. ACKNOWLEDGMENTS

The authors wish to acknowledge that this work has been partially supported by Ministry of National Defense through the Agency for Defense Development, and the author partially supported by BK21 program from Ministry of Education, Republic of Korea.

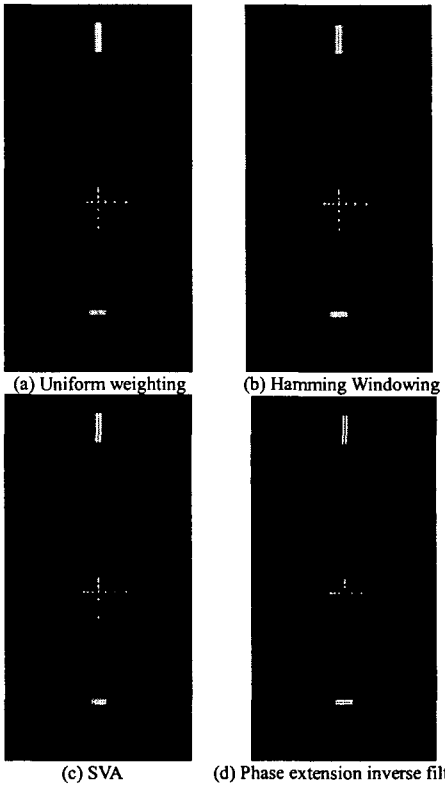

(a) Uniform weighting (b) Hamming Windowing

(c) SVA (d) Phase extension inverse filtering

Fig. 7. Uniform weighted SAR image and images produced by Hamming weighting, SVA, and the phase extension inverse filtering. The SNR_{raw} is 18.84 dB.

REFERENCES

[1] J. C. Curlander and R. N. Mcdonough, *Synthetic Aperture Radar : System & Signal Processing*, Jonh-Wiley & Sons, Inc., 1991.

[2] D. C. Munson, JR and R. L. Visentin: "A signal processing view of strip-mapping synthetic aperture radar," IEEE Trans. on Acoust., Speech, Signal Processing, vol. 37, pp. 2131-2147, Dec. 1989.

[3] S. R. DeGraaf: "SAR imaging via modern 2-D spectral estimation methods," IEEE Trans. on Image Processing, vol. 7, pp. 729-761, May. 1998.

[4] S. R. DeGraaf: "Sidelobe reduction via adaptive FIR filtering in SAR imagery," IEEE Trans. on Image Processing, vol. 3, pp. 292-301, May. 1994.

[5] H. C. Stankwitz and M. R. Kosek: "Super-resolution for SAR/ISAR RCS measurement using spatially variant apodization," Proc. AMTA Symp., Will-iamsburg, VA, pp. 251-256, Nov. 1995.

[6] Jian Li and P. Stoica: "An adaptive filtering approach to spectral estimation and SAR imaging," IEEE Trans. on Signal Processing, vol. 44, no. 6, pp. 1469-1484, Jun. 1996.

[7] H. C. Stankwitz, R. J. Dallaire, and J. R. Fienup: "Nonlinear apodization sidelobe control in SAR imagery," IEEE Trans. on Aerosp., Electronic Systems , vol. 31, pp. 267-279, Feb. 1982.